Characteristic Impedance Model for Plasmonic Metal Slot Waveguides

Dany-Sebastien Ly-Gagnon, *Member, IEEE*, Sukru Ekin Kocabaş, *Member, IEEE*, and David A. B. Miller, *Fellow, IEEE*

***Abstract*—We investigate the transmission properties of a subwavelength plasmonic slot waveguide. We show that the transmission can be accurately calculated using the characteristic impedance of the propagating mode. Using such a model, we show that it is possible to design devices without extensive 3-D Finite-difference time-domain (FDTD) computer simulations. We illustrate the approach with calculations of an asymmetric Fabry–Perot germanium photodetector based on the slot waveguide geometry, showing predicted detector efficiencies as high as 69% despite metallic losses.**

***Index Terms*—Optical planar waveguide components, photodetectors, plasmons.**

I. Introduction

INTEGRATED photonic components that allow propagation of an optical mode at subwavelength size scales are expected to play an important role in bridging the gap between optics and electronics in highly integrated optoelectronic circuits. The properties of propagating modes have recently been investigated for several plasmonic structures, such as the metal nanowire [1]–[3], metal nanoparticle arrays [4]–[6], and metal slot waveguides [7]–[10]. In particular, metal slot plasmonic waveguides were shown to support guided modes with high confinement at infrared wavelengths [7]–[10]. Such structures seem promising for guiding into subwavelength nanoscale photodetectors, as they support a high integration density and propagation lengths in the range of a few microns.

In design of optoelectronic circuits based on this geometry, it is desirable to calculate the transmission and reflection properties when waveguides with different parameters are connected together. The coupling between waveguides of different geometries has recently been studied for 2-D plasmonic waveguides of various geometries [11]–[14] and 3-D metal strips [15], [16]. However, the design of complex 3-D structures typically requires extensive computational efforts with computer-aided tools such as the finite-difference time-domain (FDTD) method.

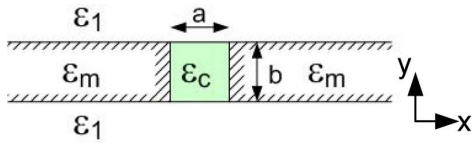

Fig. 1. Metal slot plasmonic waveguide cross section where light propagates in the z-direction.

In this paper, we investigate the transmission and reflection properties of the guided modes in metal slot plasmonic waveguides in propagation through a series of waveguide sections with different core materials. Fig. 1 shows a cross section of a metal slot plasmonic waveguide structure where the region indicated by ε_m is metal, ε_1 and ε_c are both dielectrics. This waveguide supports a bound mode where light propagates in the z-direction (normal to the plane of the figure). We show that a model that uses the characteristic impedances of different sections together can be used to calculate the transmission and reflection properties of such waveguides, even though the metal properties are quite different from those of similar guides in the microwave regime and significant loss must be included in the analysis. We then show that this model allows the design of complex waveguide structures with desired properties at a minimal computational effort by applying this technique in design of a photodetector based on an asymmetric Fabry–Perot resonator embedded in the waveguide.

II. Characteristic Impedance Model

We use a transfer matrix approach that relies on the impedance of the mode to describe the behavior of the fields as they propagate through a series of different waveguides. We note that this model is analogous to the mode-matching approach in microwaves where multiple modes might be considered [17], [18]. However, in the case of the slot waveguide, there exists a range of parameters where the waveguide supports only one bound propagating mode. For such structures, it is possible to use a transfer matrix to relate the coefficients of the forward and backward versions of the propagating mode in a linear fashion, along with the transmission and reflection coefficients at each of the discontinuities along the propagation direction.

Considering only the fundamental mode of each waveguide, we build a network model for the propagation of the fields throughout the whole structure. Applying the boundary conditions of continuity of the tangential electric and magnetic fields

Manuscript received September 7, 2007; revised November 5, 2007. First published April 11, 2008; current version published December 24, 2008. This work was supported in part by the Air Force Office of Scientific Research (AFOSR) Chip Scale Surface Plasmon Enabled Nano Structures Multidisciplinary University Research Initiatives (MURI), in part by the Focus Center Research Program/Defense Advanced Research Projects Agency (FCRP/DARPA) Interconnect Focus Research Center, and in part by the DARPA Microsystems Technology Office (MTO). The work of D.-S. Ly-Gagnon is supported by a Sequoia Capital Stanford Graduate Fellowship.

The authors are with the Ginzton Laboratory, Stanford University, Stanford, CA 94305-4088 USA (email: dalyx@stanford.edu; kocabas@ieee.org; dabm@ee.stanford.edu).

Color versions of one or more of the figures in this paper are available online at http://ieeexplore.ieee.org.

Digital Object Identifier 10.1109/JSTQE.2008.917534

reduces to

$$(A_i + B_i) = C_{i,i+1}(A_{i+1} + B_{i+1}) \tag{1a}$$

$$\frac{(A_i - B_i)}{Z_i} = C_{i,i+1}\frac{(A_{i+1} - B_{i+1})}{Z_{i+1}} \tag{1b}$$

where A_i and B_i are the amplitudes of the forward and backward propagating modes, respectively. Elements with subindex i are located before the junction (i.e., to the left of the junction for waves incident from the left), while those with subindex $(i+1)$ are located after the junction. Z_i is the characteristic impedance of the waveguide. $C_{i,i+_1}$ is the coupling coefficient that can be calculated by the mode overlap at the junction of the waveguides as

$$C_{i,i+1} = \int_S \vec{e}_{i+1} \times \vec{h}_i \cdot \hat{n}\, dS \tag{2}$$

where $\vec{e}_i$ and $\vec{h}_i$ is the normalized tangential electrical field in the ith cross section, respectively, $\hat{n}$ is the propagation direction, S is the entire cross section of the junction, and it is assumed for our model that

$$\frac{\int_S \vec{e}_{i+1} \times \vec{h}_i \cdot \hat{n}\, dS}{\int_S \vec{e}_i \times \vec{h}_{i+1} \cdot \hat{n}\, dS} \approx \frac{Z_{i+1}}{Z_i}. \tag{3}$$

For the structures under investigation, we find from simulations that this approximation is valid to about 5%.

The fields are normalized such that

$$\int_S \vec{e}_i \times \vec{h}_i \cdot \hat{n}\, dS = 1. \tag{4}$$

At the junction between two waveguide cross sections, we obtain a transfer matrix $T_{i,i+_1}$ that relates the forward and backward propagating modes as

$$\begin{bmatrix} A_i \\ B_i \end{bmatrix} = \begin{bmatrix} 1/\tau & \rho/\tau \\ \rho/\tau & 1/\tau \end{bmatrix} \begin{bmatrix} A_{i+1} \\ B_{i+1} \end{bmatrix} = \begin{bmatrix} T(1,1) & T(1,2) \\ T(2,1) & T(2,2) \end{bmatrix} = T_{i,i+1} \tag{5}$$

where

$$\tau = \frac{2Z_{i+1}C_{i,i+1}^{-1}}{Z_i + Z_{i+1}} \tag{6a}$$

$$\rho = \frac{Z_{i+1} - Z_i}{Z_i + Z_{i+1}}. \tag{6b}$$

The impedance of the mode is related to the effective permittivity ε_{eff} and the propagation constant γ by

$$Z_i = \sqrt{\frac{\mu}{\varepsilon_{\text{eff},i}}} = \frac{j\omega\mu}{\gamma_i}. \tag{7}$$

In lossy waveguides, the propagation constant $\gamma = \alpha + j\beta$ is complex, and so, the characteristic impedance of the waveguide is also complex.

The propagation through a waveguide of length L can be modeled (for the specific approach, we take later of calculating from the "right" to "left" in the structure) as

$$P_i = \begin{bmatrix} \exp(\gamma L_i) & 0 \\ 0 & \exp(-\gamma L_i) \end{bmatrix}. \tag{8}$$

Several sections of waveguides can be modeled by a transfer matrix analogous to that of a standard transmission line by alternating junction matrices and propagation matrices as

$$\begin{bmatrix} A_i \\ B_i \end{bmatrix} = T_{i,i+1}P_{i+1}T_{i+1,i+2}P_{i+2}\cdots T_{i+n-1,i+n}\begin{bmatrix} A_{i+n} \\ B_{i+n} \end{bmatrix} = T_{i,i+n}\begin{bmatrix} A_{i+n} \\ B_{i+n} \end{bmatrix}. \tag{9}$$

Thus, by knowing the propagation constants of a given waveguide section, the transmission properties of an arbitrary waveguide can be calculated.

III. Numerical Models

We used a 2-D full vectorial mode-solving approach as proposed by Lusse *et al.* [19] to solve for the properties of the actual propagating modes in each waveguide where the properties of materials are different, hence obtaining the necessary parameters to use in transfer matrix methods. With appropriate initial conditions, these calculations can be executed in a few minutes on a personal computer.

We also used FDTD simulations to verify the values of the propagation constants obtained by the mode-solving approach [20]. The FDTD uses magnetic and electric walls at symmetry planes to reduce the computation effort. Convolution perfectly matched layers (C-PMLs) surround the structure in all directions. For these simulations, the guide is excited by a magnetic dipole located in the core region of the waveguide with a sinusoidal signal wrapped in a Gaussian envelope.

Our study focuses on gold as the metal. We model the gold as a Drude metal and its permittivity is given as

$$\varepsilon(\omega) = 1 - \frac{\omega_p^2}{\omega^2 + i\gamma_p\omega} \tag{10}$$

where $\omega_p = 1.204 \times 10^{16}$ rad/s and $\gamma_p = 1.375 \times 10^{14}$ rad/s [21].

The propagation constants from the FDTD were calculated by observing the phase variation and the decay of the mode along the propagation direction. While no attempt was made to mitigate numerical dispersion in the grid, we found a difference in propagation constant of less than 2% between the FDTD and the mode-solving approach. To minimize numerical artifacts in comparing our transfer matrix results to the full FDTD simulations of the structure, we used the propagation constants from the FDTD simulations in calculations involving the impedance model, though we believe, given the agreement between the two approaches, that the faster mode-solving approach is otherwise generally sufficient.

The effective refractive index n_{eff} is related to the imaginary part of the propagation constant γ as $n_{\text{eff}} = \beta c/\omega$. The propagation length L_p is defined as the length for which the field intensity attenuates by a factor of $(1/e)$ and is related to the real part of the propagation constant γ as $L_p = 1/2\alpha$. The surrounding material was silicon dioxide for all simulations with a refractive index of 1.44. The dimensions of the waveguide core ($a \times b$) were 80 nm $\times$ 80 nm (see inset in Fig. 2). The core of the waveguide was filled with silicon dioxide, silicon,

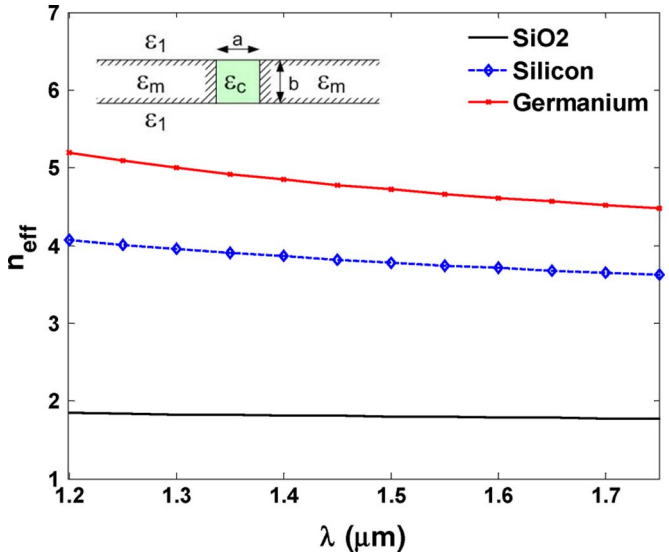

Fig. 2. Effective refractive index for different filling materials in the core. The inset represents the cross section of the slot waveguide structure. The core region has permittivity ε_c. (The germanium loss is taken as that at 1.3 μm).

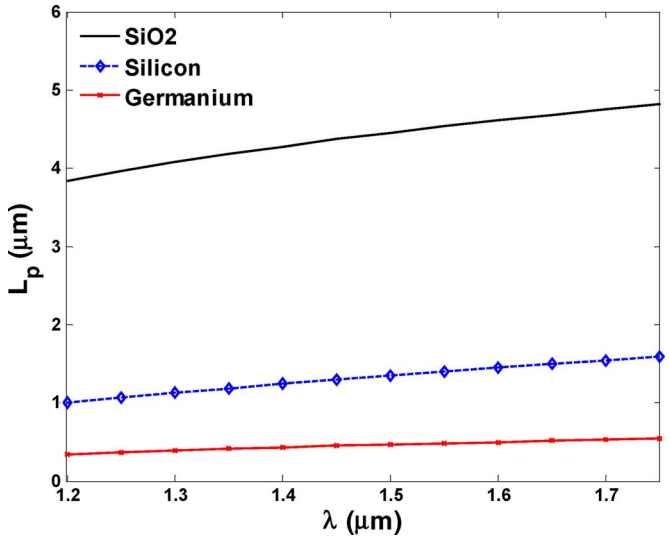

Fig. 3. Propagation length for waveguides with different filling materials in the core. (The germanium loss is taken as that at 1.3 μm).

or germanium. Silicon was taken to have a refractive index of 3.52. Germanium was modeled with a complex refractive index of $4.23 + 7.8 \times 10^{-2} j$, which corresponds to a power loss absorption coefficient of $\alpha_G = 7540\ \mathrm{cm}^{-1}$ [22]. (For simplicity of simulation, the germanium loss was taken independently of frequency, though the loss does drop off relatively abruptly for wavelengths longer than $\sim$1.5 μm, and there is a slow rise for wavelengths progressively shorter than $\sim$1.5 μm. This particular loss number is characteristic of germanium at a wavelength of 1.3 μm).

The propagation constants found with the mode-solving approach for the slot waveguides with different materials filling the core are shown in Figs. 2 and 3. For these dimensions, there exist only one propagating bound mode above cutoff. This mode is quasi-TEM with dominant H_y and E_x fields, i.e., the electric

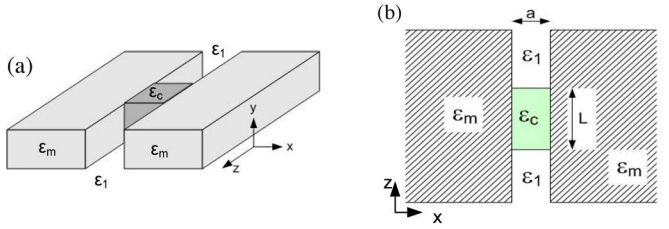

Fig. 4. Fabry–Perot structure. (a) Perspective view of the structure. (b) Top view of the structure.

field is primarily polarized "horizontally" from one strip to the other and the magnetic field is primarily vertical (see Fig. 1 for coordinate directions).

IV. Reflection from a Fabry–Perot Structure

As a specific structure of interest also for potential applications, e.g., in photodetectors, we consider first a single-slab Fabry–Perot structure embedded in a plasmonic slot waveguide. The structure is shown in Fig. 4. It consists of a slot waveguide where the core region has a different permittivity ε_c for a given length L. The dimensions of the waveguide are $(a \times b) =$ 80 nm $\times$ 80 nm. The metal used is gold, and extends to infinity in the positive and negative x-directions. The ambient material is silicon dioxide, with a refractive index of 1.44. The waveguide core region is filled with silicon of length varying between 100 and 800 nm. The refractive index of silicon was taken as 3.52, and the silicon is presumed lossless in this simulation. We examined the calculated power reflected from the structure as we varied the cavity length L.

The power reflected at the front surface of the silicon in a full FDTD simulation of this structure was deduced from the standing wave electrical field amplitudes. We use the absolute value of the electric field at position $z = z_{\max}$, where it has a maximum amplitude, and at position $z = z_{\min}$, where it has minimum amplitude (assuming propagation in the forward z-direction and $z = 0$ as the front surface of the silicon). We find the reflected power using the ratio of the maximum electric field $|E|_{\max}$ at position $z_{\max}$ and the minimum electric field $|E|_{\min}$ at position $z_{\min}$. Defining this ratio as

$$R = \frac{|E|_{\max}}{|E|_{\min}} \tag{11}$$

the reflected power is given as

$$|\rho| = \frac{R \exp\left(-z_{\min}/2L_p\right) - \exp\left(-z_{\max}/2L_p\right)}{R \exp\left(z_{\min}/2L_p\right) + \exp\left(z_{\max}/2L_p\right)} \tag{12}$$

where L_p is the propagation length for a silicon dioxide core waveguide.

We calculated the reflected power expected from the impedance model as

$$|\rho|^2 = \left|\frac{T(2,1)}{T(1,1)}\right|^2. \tag{13}$$

We compare the results of the FDTD simulations to those from the characteristic impedance model. Fig. 5 presents the

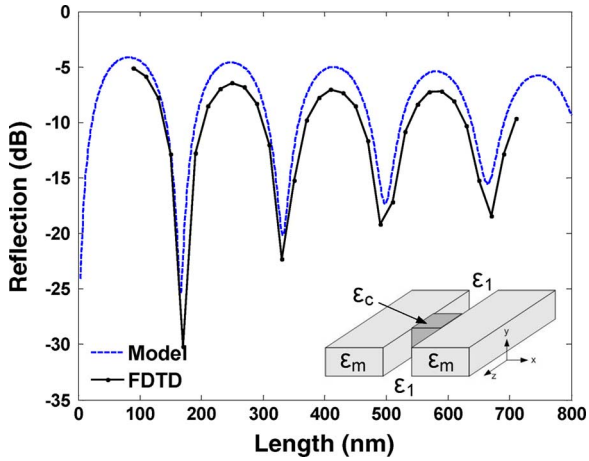

Fig. 5. Reflected power from a Fabry–Perot structure at $\lambda = 1.3$ μm as a function of the length of the silicon core section.

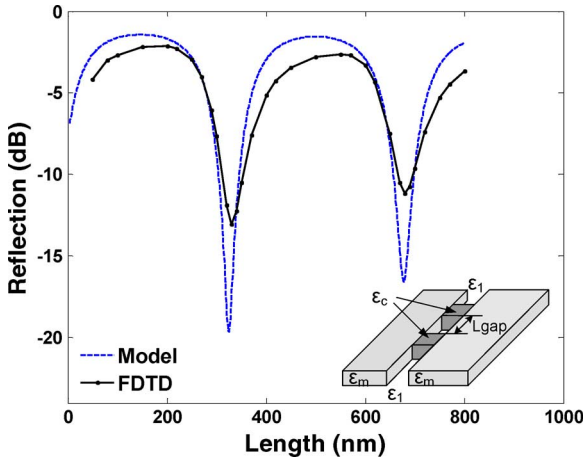

Fig. 7. Reflection spectrum of two coupled Fabry–Perot resonators at $\lambda = 1.3$ μm as a function of their separation distance L_{gap}.

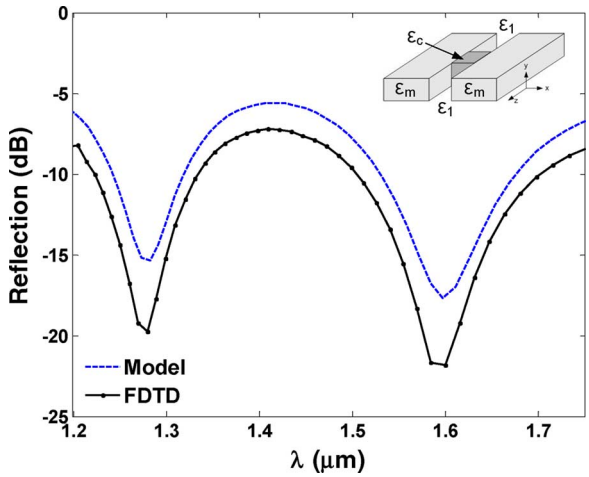

Fig. 6. Reflection spectrum of a Fabry–Perot resonator for a length of 650 nm.

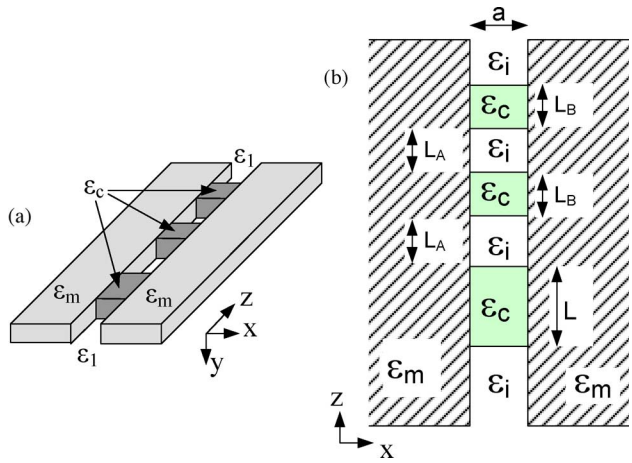

Fig. 8. Asymetric Fabry–Perot structure. (a) Perspective view. (b) Top view.

reflection as a function of length for a wavelength of 1.3 μm. In Fig. 6, we show the reflected spectrum as a function of wavelength in a cavity length L of 650 nm. We note that the reflection as calculated from the characteristic impedance model well describes the behavior of the device. The reflection measured in FDTD simulation was a few decibels lower than what was calculated by the impedance model. This discrepancy can be explained by presuming that power is also coupled into radiation modes and higher order modes below cutoff that are excited at the discontinuities and that were not taken into consideration in our single-mode transfer matrix impedance model.

We calculated the reflection from a structure with two separate pieces of silicon within the guide as a function of their separation distance L_{gap}. In this case, the pieces of silicon are effectively operating as mirrors, forming a Fabry–Perot resonator between them, a resonator that should tune as this separation distance is varied. The two pieces of silicon have the same cross-sectional dimensions (80 nm $\times$ 80 nm) and are each 100 nm long. The reflection at 1.3 μm as a function of the separation length between the two cavities is shown in Fig. 7. The model well describes the reflection of the structure to a few decibels, and again, we expect that the difference between the model and the FDTD simulations may be the result of radiation modes that are neglected in the model.

This transfer matrix model based on the calculated complex mode impedance of the plasmonic metal slot guides, thus offers a useful approach at a greatly reduced computing cost compared to full FDTD simulations of the structure.

V. Design of Structures Using the Characteristic Impedance Model

We can apply the impedance model to design a germanium-based photodetector at 1.3 μm. The design consists of an asymmetric Fabry–Perot resonator using the first piece of germanium as the front reflector and the primary absorbing region, followed by a back reflector that is designed by alternating different elements of germanium with silicon dioxide spacers, nominally in the form of a Bragg reflector structure (see Fig. 8).

The structure had the same cross section as the one depicted in Fig. 2, with dimensions $a \times b$ of 80 nm $\times$ 80 nm. We used SiO_2 as the surrounding material, with refractive index of 1.44. At 1.3 μm, the germanium has a complex refractive

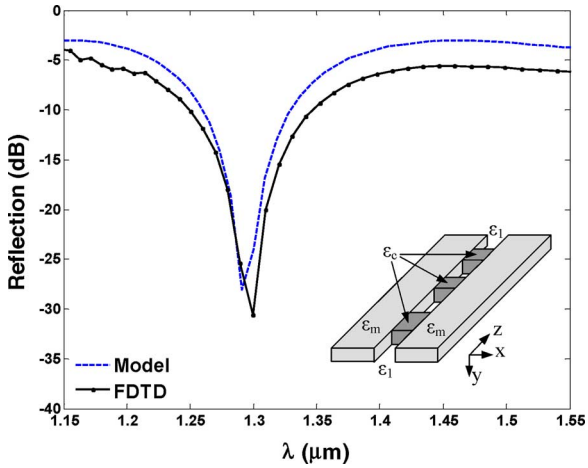

Fig. 9. Reflection at the front surface of an asymmetric Fabry–Perot structure for a photodetector length L of 260 nm.

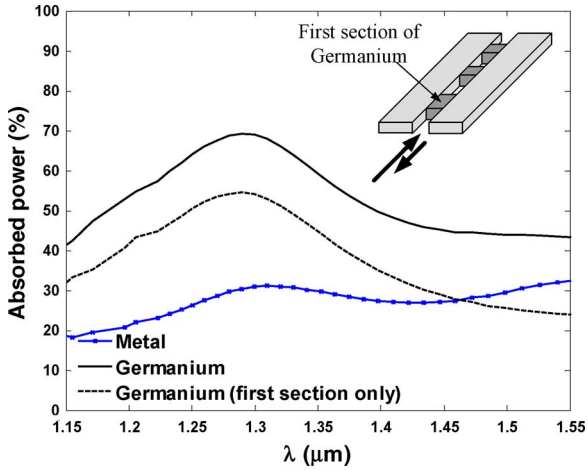

Fig. 10. Absorbed power in the asymmetric Fabry–Perot photodetector. (The germanium loss is taken as that at 1.3 μm).

index of $4.23 + 7.8 \times 10^{-2} j$, which corresponds to a power loss absorption coefficient in bulk germanium of $\alpha_G = 7540$ cm^{-1} as before.

The back reflector was designed by considering unit cells of the Bragg reflector structure. The unit cell consists of a cross section with silicon dioxide in the core for a propagation length of L_A, followed by a similar structure but filled in the core with germanium for a propagation length of L_B. The unit cell was designed such that no field would propagate through the entire structure if the unit cell were repeated a large number of times. For the given refractive indexes of silicon dioxide and germanium, a length of 190 nm for both L_A and L_B would create a Bragg back reflector at 1.3 μm.

Using the characteristic impedance model, we then calculated the length of the photodetector L that would maximize the absorbed power in this cross section. For a length of 260 nm, the impedance model shows that the amount of reflected power is less than 1% when two unit cells are used as the Bragg back reflector (as in Fig. 8). The amount of power reflected from the asymmetric Fabry–Perot as a function of the wavelength is shown in Fig. 9. We note that the model correctly predicts the shape of the reflection spectrum and its minimal value at 1.3 μm. The FDTD simulations also showed a reflected power of less than 1% at that wavelength.

The amount of power absorbed in this device by different portions of the structure is shown in Fig. 10, as calculated by the FDTD. There are two loss mechanisms in this structure: the loss due to attenuation of the propagating fields in the metal and the absorption in the germanium semiconductor that contributes to photocurrent. The fraction of power absorbed into a given volume can be calculated from the power flowing into this closed surface less the power flowing out of it.

At 1.3 μm, 30.9% of the power was absorbed in the metal past the front surface. The germanium elements, which represent a volume of 4.1×10^{-3} μm^3 absorbed 69.05% of the total power. The first section of germanium, which consists of a cube of 80 nm $\times$ 80 nm $\times$ 260 nm absorbed 54.1% of the incoming power. Also, the absorption peak occurs at 1.3 μm, where the photodetector was designed to operate. Assuming full quantum efficiency, this detector would have a responsivity of 0.72 A/W at 1.3 μm.

Such a device could be fabricated from germanium on insulator wafers by first patterning the germanium, and subsequently, depositing metal with a liftoff process. The two metal stripes on each side of the germanium could be used to bias the photodetector and create a metal–semiconductor–metal junction. Light could be coupled at the end of the device by a dielectric waveguide or an optical fiber, or by a nanometallic scatterer located close to the waveguide, though such coupling mechanisms remain subject for further investigation.

VI. Conclusion

We presented a simple model to account for the transmission properties of a plasmonic metal slot waveguide with discontinuities in the propagation direction. We showed that this model accurately modeled the properties of interconnected slot waveguides with different materials filling the core region. This model can be readily applied to design structures without extensive time-domain simulations. As an example, we designed an asymmetric Fabry–Perot waveguide photodetector with minimal front surface reflection. The designed photodetector absorbed 69% of the incident power in a volume 4.1×10^{-3} μm^3. We also, therefore, conclude that useful nanoscale photodetectors will be possible by such techniques, and we expect that such devices would have a large electrical operating bandwidth due to their physical size and a corresponding small capacitance.

Acknowledgment

The authors would like to thank G. Veronis for useful discussions. They also thank the anonymous reviewers for their valuable comments.

References

[1] P. Berini, "Plasmon polariton modes guided by a metal film of finite width," *Opt. Lett.*, vol. 24, no. 15, pp. 1011–1013, Aug. 1999.

[2] J.-C. Weeber, A. Dereux, C. Girard, J. R. Krenn, and J.-P. Goudonnet, "Plasmon polaritons of metallic nanowires for controlling submicron propagation of light," *Phys. Rev. B*, vol. 60, no. 12, pp. 9061–9068, 1999.
[3] R. Zia, A. Chandran, and M. L. Brongersma, "Dielectric waveguide model for guided surface polaritons," *Opt. Lett.*, vol. 30, no. 12, pp. 1473–1475, Jun. 2005.
[4] M. L. Brongersma, J. W. Hartman, and H. A. Atwater, "Electromagnetic energy transfer and switching in nanoparticle chain arrays below the diffraction limit," *Phys. Rev. B*, vol. 62, no. 24, pp. R16356–R16359, Dec. 2000.
[5] J. R. Krenn, "Light field propagation by metal micro- and nanostructures," *J. Microsc.*, vol. 202, pp. 122–128, Apr. 2001.
[6] S. A. Maier, P. G. Kik, H. A. Atwater, S. Meltzer, E. Harel, B. E. Koel, and A. A. Requicha, "Local detection of electromagnetic energy transport below the diffraction limit in metal nanoparticle plasmon waveguides," *Nat. Mater.*, vol. 2, no. 4, pp. 229–232, Apr. 2003.
[7] G. Veronis and S. Fan, "Guided subwavelength plasmonic mode supported by a slot in a thin metal film," *Opt. Lett.*, vol. 30, no. 24, pp. 3359–3361, Dec. 2005.
[8] L. Liu, Z. Han, and S. He, "Novel surface plasmon waveguide for high integration," *Opt. Exp.*, vol. 13, no. 17, pp. 6645–6650, Aug. 2005.
[9] J. A. Dionne, H. J. Lezec, and H. A. Atwater, "Highly confined photon transport in subwavelength metallic slot waveguides," *Nano Lett.*, vol. 6, no. 9, pp. 1928–1932, 2006.
[10] R. Zia, M. D. Selker, P. B. Catrysse, and M. L. Brongersma, "Geometries and materials for subwavelength surface plasmon modes," *J. Opt. Soc. Am. A*, vol. 21, no. 12, pp. 2442–2446, Dec. 2004.
[11] G. Veronis and S. Fan, "Bends and splitters in metal-dielectric-metal subwavelength plasmonic waveguides," *Appl. Phys. Lett.*, vol. 87, no. 13, pp. 131102-1–131102-3, 2005.
[12] T.-W. Lee and S. Gray, "Subwavelength light bending by metal slit structures," *Opt. Exp.*, vol. 13, no. 24, pp. 9652–9659, Nov. 2005.
[13] G. Veronis and S. Fan, "Theoretical investigation of compact couplers between dielectric slab waveguides and two-dimensional metal-dielectric-metal plasmonic waveguides," *Opt. Exp.*, vol. 15, no. 3, pp. 1211–1221, Feb. 2007.
[14] I. Breukelaar and P. Berini, "Long range surface plasmon polariton mode cutoff and radiation in slab waveguides," *J. Opt. Soc. Amer. A*, vol. 23, no. 8, pp. 1971–1977, Jan. 2006.
[15] R. Charbonneau, C. Scales, I. Breukelaar, S. Fafard, N. Lahoud, G. Mattiussi, and P. Berini, "Passive integrated optics elements based on long-range surface plasmon polaritons," *J. Lightw. Technol.*, vol. 24, no. 1, pp. 477–494, Jan. 2006.
[16] I. Breukelaar, R. Charbonneau, and P. Berini, "Long-range surface plasmon-polariton mode cutoff and radiation in embedded strip waveguides," *J. Appl. Phys.*, vol. 100, pp. 043104-1–043104-9, 2006.
[17] A. Wexler, "Solution of waveguide discontinuities by modal analysis," *IEEE Trans. Microw. Theory Tech.*, vol. MTT-15, no. 9, pp. 508–517, Sep. 1967.
[18] F. Arndt, J. Brandt, V. Catina, J. Ritter, I. Rullhusen, J. Dauelsberg, U. Hilgefort, and W. Wessel, "Fast CAD and optimization of waveguide components and aperture antennas by hybrid MM/FE/MoM/FD methods," *IEEE Trans. Microw. Theory Tech.*, vol. 52, no. 1, pp. 292–305, Jan. 2004.
[19] P. Lusse, P. Stuwe, J. Schule, and H. G. Unger, "Analysis of vectorial mode fields in optical waveguides by a newfinite difference method," *IEEE J. Lightw. Tech.*, vol. 12, no. 3, pp. 487–494, Mar. 1994.
[20] A. Taflove and S. Hagness, *Computational Electrodynamics: The Finite-Difference Time-Domain Method*, 3rd ed. Boston, MA: Artech House, 2005.
[21] E. D. Palik, *Handbook of Optical Constants of Solids*. New York: Academic, 1985.
[22] S. Adachi, *Optical Constants of Crystalline and Amorphous Semiconductors: Numerical Data and Graphical Information*. New York: Springer-Verlag, 1999.

Dany-Sebastien Ly-Gagnon received the B.S. degree in electrical engineering from Ecole Polytechnique of Montreal, Montreal, Canada, and the M.S. degree in electronics engineering from the University of Tokyo, Tokyo, Japan, in 2002 and 2004, respectively. He is currently working toward the Ph.D. degree in electrical engineering at Stanford University, Stanford, CA.

His current research interests include optical transmission systems and optoelectronic devices for optical interconnects.

Sukru Ekin Kocabas (M'00) received the B.S. degree from Bilkent University, Ankara, Turkey, in 2002 and the M.S. degree in 2004 from Stanford University, Stanford, CA, both in electrical engineering, where he is currently working toward the Ph.D. degree majoring in electrical engineering with a minor in physics.

His current research interests include modeling and fabrication of nanophotonic optoelectronic devices.

David A. B. Miller (M'84–SM'89–F'95) received the B.Sc. degree from St. Andrews University, St. Andrews, U.K., in 1976, and the Ph.D. degree from Heriot–Watt University, Edinburgh, U.K., in 1979, both in physics.

From 1981 to 1996, he was with Bell Laboratories, Murray Hill, NJ, as a Department Head. During 1997–2006, he was the Director of the Ginzton Laboratory, Stanford University, Stanford, CA, where he is currently the W. M. Keck Professor of Electrical Engineering, the Director of the Solid State and Photonics Laboratory, and the Co-Director of the Stanford Photonics Research Center. He is the author or coauthor of more than 200 scientific papers and delivered more than 100 conference invited talks. He holds 62 patents. His current research interests include nanophotonic and quantum-confined optoelectronic physics and devices, and fundamentals and applications of optics in information sensing, switching, and processing.

Dr. Miller was a Board Member for both the Optical Society of America (OSA) and the IEEE Lasers and Electro-Optics Society (LEOS), and in various other societies and conference committees. He was the President of the IEEE Lasers and Electro-Optics Society in 1995. He was the recipient of Adolph Lomb Medal and the R.W. Wood Prize from the OSA, the International Prize in Optics from the International Commission for Optics, and the IEEE Third Millennium Medal. He is a Fellow of the Royal Societies of London and Edinburgh, the OSA, and the American Physical Society (APS). He holds honorary degrees from the Vrije Universiteit Brussel and Heriot–Watt University.